# SESSION III

Session Chairperson
A.M.O. SMITH

*University of California at Los Angeles*
*Los Angeles, California*

# THE EFFECT OF BASE SLANT ON THE FLOW PATTERN AND DRAG OF THREE-DIMENSIONAL BODIES WITH BLUNT ENDS

T. MOREL

*General Motors Research Laboratories, Warren, Michigan*

## ABSTRACT

The paper describes an experimental investigation concerning the effects of slanting the blunt base of three-dimensional bodies having either an axisymmetric or a rectangular cross section. It was found that base slant can have a very dramatic effect on body drag, particularly in a relatively narrow range of slant angles where the drag coefficient exhibits a large local maximum (overshoot).

Detailed study of the flow showed that the drag maximum is related to the existence of two very different separation patterns at the rear of either body. One pattern is similar to that found behind axisymmetric bodies with no base slant, and its main feature is the presence of a closed separation region adjacent to the base. The other pattern is highly three-dimensional with two streamwise vortices approximately parallel to the slanted surface, one at each side of the body. The drag coefficient maximum occurs in the slant-angle range where a changeover from one flow pattern to the other takes place. The observed phenomenon may be thought of as being associated with a broader category of "critical geometries," which is tentatively defined and discussed.

## NOTATION

| | |
|---|---|
| A | projected frontal area |
| AR | aspect ratio of the slanted surface; width/length |
| $C_D$ | drag coefficient $\equiv$ drag force/($\rho$/2 $U^2$A) |
| $C_L$ | lift coefficient $\equiv$ lift force/($\rho$/2 $U^2$A) |

*References pp. 216-217.*

| | |
|---|---|
| $C_p$ | pressure coefficient $\equiv (p - p_\infty) / \rho/2\ U^2)$ |
| $C_{pb}$ | base-pressure coefficient |
| D, d | body diameter |
| $D_{eq}$ | equivalent diameter $\equiv \sqrt{4\ \text{area}/\pi}$ |
| H,h | height |
| $\ell$ | body dimension in the stream direction |
| $L_S$ | length of a slanted surface |
| p | static pressure |
| $p_\infty$ | free-stream static pressure |
| $Re_D$ | Reynolds number $\equiv$ UD/$\nu$ |
| r | radius |
| $S_D$ | Strouhal number $\equiv$ fD/U |
| t | thickness |
| U | free-stream velocity |
| u' | rms turbulence intensity |
| W | width |
| x | streamwise coordinate |
| $\alpha$ | angle of inclination of a slanted base away from the normal to the stream direction |
| $\nu$ | kinematic viscosity |
| $\rho$ | density |
| $\theta$ | momentum thickness |

## INTRODUCTION

One of the most important practical objectives of subsonic aerodynamics research is the determination of the overall pressure forces – in particular, of lift and drag. In the case of *streamlined bodies* the major interest is usually in lift, trends of which may be determined fairly well using inviscid flow models. Inviscid models can also be used to estimate the so-called "induced" drag of streamlined three-dimensional bodies with little or no separation. Other sources of pressure drag, e.g., separated regions or boundary layer displacement effects, are considerably more difficult to deal with but,

for streamlined bodies, they usually are of only secondary importance. The *bluff-body* situation, where drag rather than lift is the major unknown, stands in sharp contrast to the successful prediction of streamlined-body flows. In this case there always are extensive regions of separation generating large drag, and there is no general theoretical model that can be used for its prediction.

There is a large amount of information in the literature about the pressure drag of various bluff bodies, and also about the mechanisms by which this drag is generated. Considering this wealth of information, one may inquire whether one can develop it into the form of building blocks, from which at least the *trends* of flow pattern and force variation with changes in body geometry may be predicted. The objective would be to progress to a point where educated guesses can be made to guide experimental programs. This, indeed, was one of the major ideas behind the program of this Symposium.

While an evolution towards a capability for better prediction of the flow behavior of bluff bodies is undoubtedly taking place, there will always be a need to check bluff-body flows experimentally (physically or numerically) through systematic perturbation of the geometrical parameters, in order to find the optimum configuration for any given purpose.

One of the reasons why a continued need for systematic experiments can be expected, is the existence of what can tentatively be called "critical geometries." The concept of critical geometries, as it stands now, is meant to deal with cases where drag exhibits a local maximum with respect to some geometrical parameter of a body shape. The fact that the variation of $C_D$ with that parameter does not follow a monotonic trend creates a difficulty, since one is faced with two opposing trends and with some (unknown) critical value of the parameter at which the trends change.

A comprehensive survey of the bluff-body literature will reveal only relatively few carefully documented cases of such critical geometries. It is probable, that others may have been encountered but have not been reported for a variety of reasons, e.g., being unexpected and therefore suspect, or being of no interest to the purpose of the particular investigation and thus simply avoided. The few cases that we could identify in the bluff-body literature, and which are presented below, therefore show only some of the possible types of critical geometries that may exist.

Nash, Quincey & Callinan (1963) observed the existence of a local drag maximum on a two-dimensional body with a short splitter plate (Fig. 1). The change of trend at $\ell/h = 1$ was explained as being due to a change in flow regime, which was documented by shadow photographs showing differences in the separated shear layers in the two regimes.

*References pp. 216-217.*

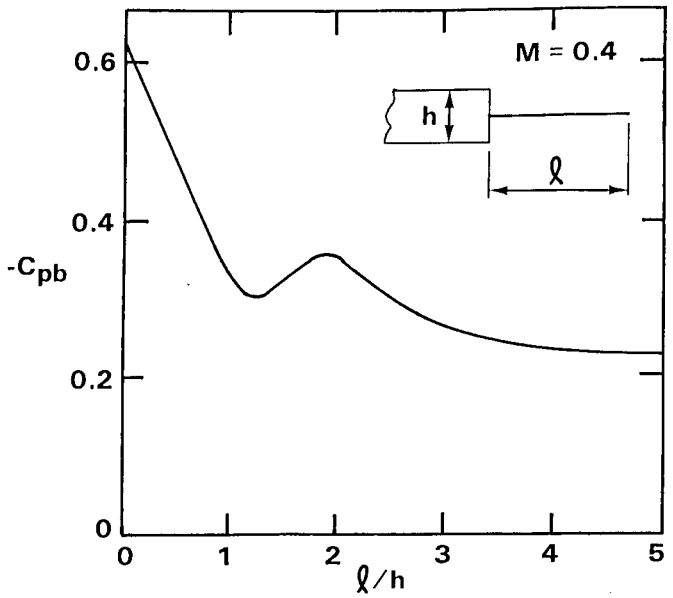


Fig. 1. Two-dimensional body with a splitter plate (Nash et al., 1963).

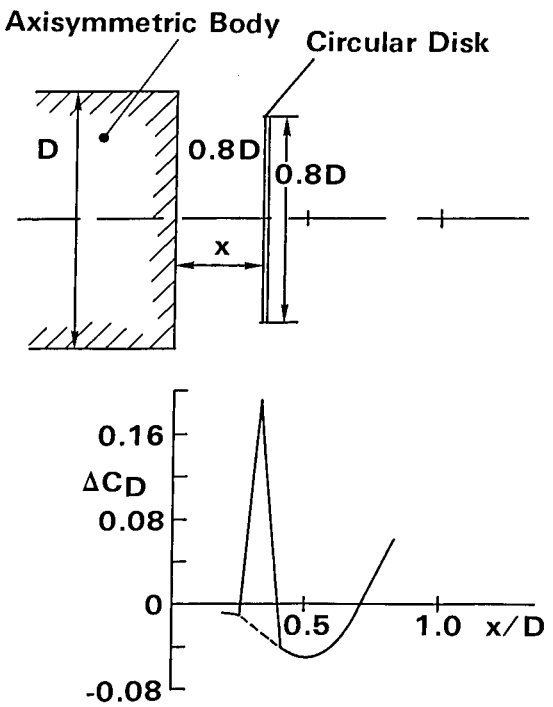


Fig. 2. Effect of a circular disk on afterbody drag, showing the occurrence of critical behavior at x/D = 0.3 (Mair, 1965).

Mair (1965) observed an unexpected drag increase while investigating the drag-reducing capability of circular disks placed concentrically in the near-wake of a blunt based body of revolution at $Re_D$ = 150,000. He found the effect of the added disks beneficial in general, particularly so for a disk with d/D = 0.8 placed at about x/D = 0.5 (Fig. 2). However, when the disk that gave the largest drag reduction was moved from its optimum position towards the base, a new flow regime was formed which was highly unsteady and produced a large drag increase; it occurred in a relatively narrow range of x/D.

Critical geometries may also be found on smooth-shaped bodies. One such case was observed by Mair (1969) in his study of the effect of boat-tailing on the drag of axisymmetric bodies, at $Re_D$ = 460,000. On three of eight boat-tails tested he noted critical boat-tail lengths at which the drag had a local maximum. Fig. 3 shows the drag curve of one of the three "critical" boat-tails, for which Mair noted: "For L/D ≈ 0.8 the drag fluctuated considerably and separation was probably occurring close to the cut-off base. For L/D < 0.65 and again L/D > 0.9, there was no unsteadiness in the drag."

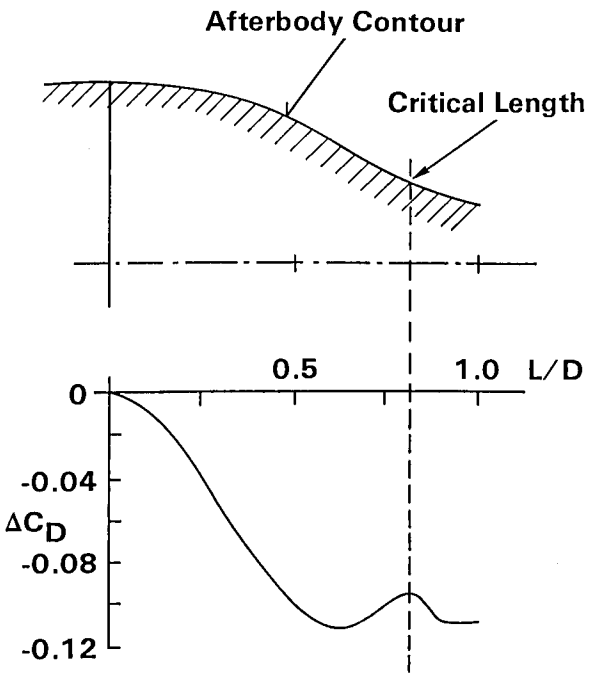


Fig. 3. Smooth-shaped afterbody exhibiting a critical behavior (Mair, 1969).

*References pp. 216-217.*

Bearman & Trueman (1972) studied one critical geometry uncovered earlier by Nakaguchi, Hashimoto & Muto (1968), with the objective of testing Bearman's vortex-street wake model. The tested bodies were rectangular 2-D bars with various thickness-to-height ratios (t/h = 0.2 - 1.2), at $Re_h$ = 2-7 x $10^4$ (Fig. 4). It was found that the drag had a local maximum at around t/h = 0.62, associated with a marked increase in the intensity of the regular vortex shedding. The magnitude of the increase was very large, with $C_D$ going from about 2 at zero thickness to about 3 at the critical thickness. The whole drag increase was shown to be due to base-pressure decrease, the forebody drag being about constant for all t/h. Addition of a splitter plate behind the rectangular body entirely eliminated this behavior, showing that vortex shedding was playing a key role in the generation of the excess drag.

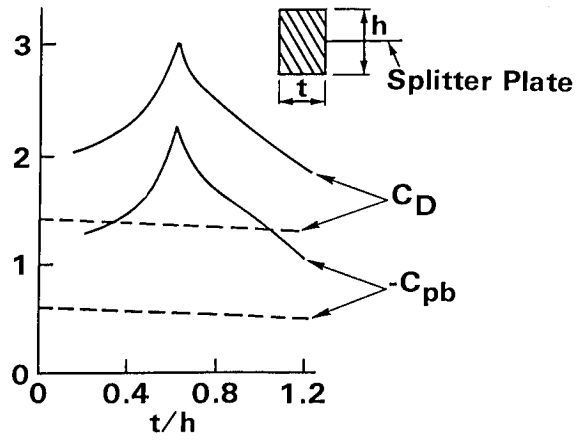


Fig. 4. Drag of 2-D rectangular bars of various thickness-to-height ratios (Bearman & Trueman, 1972).

One case of a critical geometry concerning road vehicles was documented by Janssen & Hucho (1974). Their experiment involved changes in the angle of the slanted portion of the roof of a car and their effect on drag. They observed that for a small range of roof angles (55-65°) the curve of overall drag exhibited a large overshoot (Fig. 5). They also observed a change in the extent of afterbody flow

separation in the critical range, and documented it by the two sketches included in Fig. 5. They observed that the upper separation line was at the top of the slanted surface for $\alpha < 58°$, but that it moved to the bottom for $\alpha > 62°$; in between these two angles the point of separation was seen to pulse randomly from the top to the bottom and vice versa.

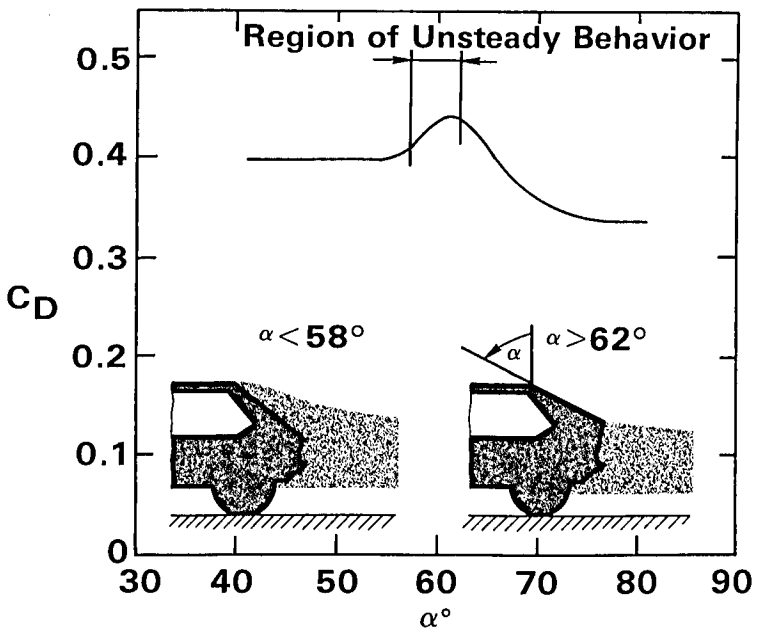


Fig. 5. Critical behavior of a hatchback automobile (Janssen & Hucho, 1974).

What do these five examples have in common? Can we consider them as one class? The definition of CG suggested earlier, which singles out the existence of a local drag maximum as the defining feature, is of a practical rather than fluid mechanical nature. It was intended to focus attention on geometries with local drag maxima mostly because they may be considered anomalous. They also have one thing in common: a small change of the critical geometrical parameter in either direction leads to a drag reduction. Since the necessary change can be in either direction, it should be feasible in many cases to avoid the high-drag region altogether. In fluid-mechanical terms the definition of CG is much more difficult. At this point the only common denominators seem to be the presence of flow separation, and the existence of two competing flow patterns. Excessive unsteadiness is often, but not always, present as well.

It is instructive to note that most of the mentioned examples of CG, if not all,

were encountered by chance with no prior expectation of the critical behavior. The fact that the drag overshoots are often unsuspected, coupled with the complex and difficult-to-analyze types of flow they tend to involve, means that one has to rely on systematic experimental studies for identification of critical geometries and for description of their behavior.

Finally, the above examples demonstrate that critical geometries can generate sizeable excess drag, and this should be of concern to designers of bluff-body hardware.

## SLANTED BASE AS ONE PARTICULAR CRITICAL GEOMETRY

Of the critical geometries mentioned, the one that attracted our attention the most was the last one, concerning the effect of base slant on body drag. The observed drag variation with slant angle was of such a magnitude as to be of considerable practical interest. Consequently, it was decided to study this problem in detail, in order to search for the limits of its operation and for the maximum drag overshoot that may be expected. In addition, it was hoped that some light could be shed on the mechanisms involved in the generation of the excess drag, thus providing guidance for efforts to control or eliminate it.

The work of Janssen & Hucho (1974) provided two early clues to what was happening. First, they reported that near the critical angle the roof separation line moved from the top of the slanted surface to its bottom edge. Second, they stated that the increase in $C_D$ was "due to strong edge vortices with a correspondingly large induced drag." Upon study of these observations we concluded that the drag overshoot found on the hatchback cars was most likely a consequence of a major change in the near-wake flow pattern. The conjecture was that below 58° the time-mean separation pattern was quasi-axisymmetric (or "closed"), with the external flow passing over a closed recirculating region adjacent to the base, in much the same manner as in the well-known cases of two-dimensional and axisymmetric base flows (Fig. 6a). Beyond 62° the picture was conjectured to have been very different; secondary flows, driven by pressure differentials from the sides of the body onto the slanted surface, rolled up upon separation from the side edges into two streamwise vortices extending into the wake. The resulting separation pattern was, thus, strongly three-dimensional and could be characterized as "open" (Fig. 6b). This type of separation is well known from delta-wing experiments. In terms of mean streamlines near the body surface, the quasi-axisymmetric pattern is one where the surface streamlines upstream of the base are approximately aligned with those expected in a potential flow, while in the 3-D case they may be substantially inclined away from the potential-flow streamlines.

The streamwise vortices appearing in the 3-D case may be expected to interact with the flow away from the edges and increase the tendency for reattachment in the

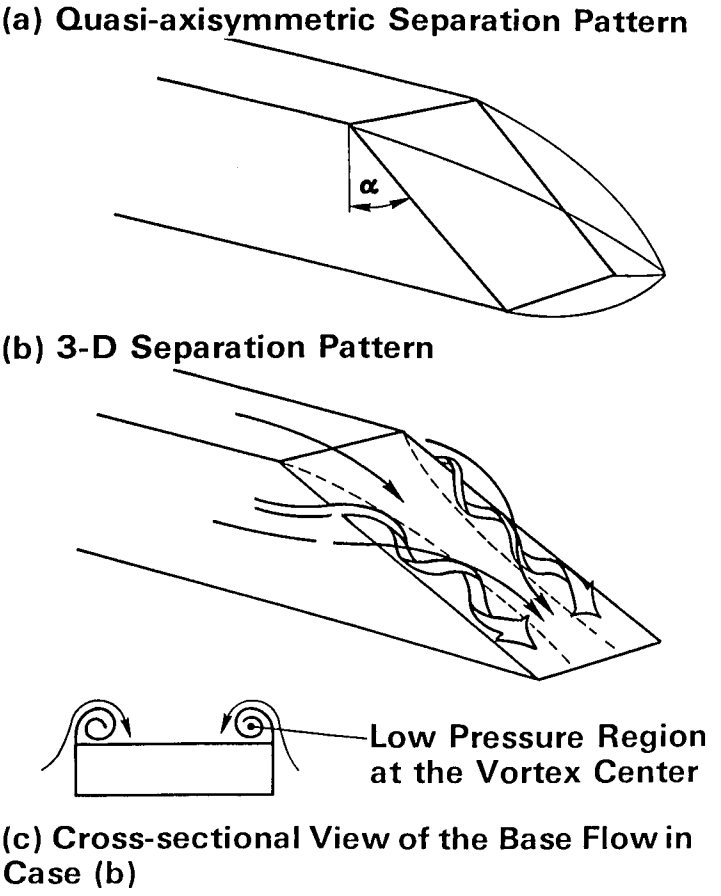


Fig. 6 Two types of separated-flow pattern on a slanted base.

central portion of the slanted surface. At first glance it may appear that such induced attachment should be beneficial from the drag point of view. However, it must be realized that the attachment need not mean that the wall flow is decelerating to the degree expected from 2-D thinking. Rather, the attached flow pattern is maintained by a supply of fluid from the sides of the body, which passes over the longitudinal vortices onto the slanted base, relieving the pressure rise along the central portion of the inclined surface. Near the side edges of this surface the wall pressure may be expected to be much lower than in the center, due to the proximity of the rolled-up streamwise vortices which may have very low pressure inside their cores. The contribution to drag which comes from these low-pressure regions is a manifestation

*References pp. 216-217.*

of the energy which is being continuously supplied into the edge-vortices. There is a contrast between the large separated region of almost uniform low pressure on the one hand, and the discrete vortices and localized very-low pressure regions on the other. Thus, from the drag point of view, the relative merits of the quasi-axisymmetric and 3-D separation are not immediately obvious and can be resolved only by experiments.

From a practical point of view, the critical-angle range should be avoided in situations where low drag is a high-priority design objective. However, since it may not always be possible to avoid this critical-angle range, one wonders whether small modifications to the body shape may be sufficient to suppress the drag overshoot. The answer to this question should be facilitated by a better understanding of the phenomena involved, and this was one of the main objectives of the investigation that is reported here.

## SLENDER AXISYMMETRIC CYLINDER WITH SLANTED BASE

The details of the critical behavior of a slanted base, the amount of drag overshoot and the value of the critical angle may all be expected to depend on a number of parameters, for example: aspect ratio of the slanted surface, geometry of the afterbody, geometry of the forebody, ground proximity and Reynolds number. It is evident that no single experiment can answer all questions, and so one must seek a compromise. The most important question for this investigation was whether the conjecture about the flow patterns was correct, and so the first experiment was designed specifically so that all changes in the flow could be ascribed to the base slant angle alone.

The study concerned itself with the case where a base is preceded by a finite forebody. Because variation of the slant angle causes changes in the overall length/diameter ratio ($\ell$/D), a rather long and slender body configuration with $\ell$/D = 9 was used to minimize this effect. The large $\ell$/D also reduced the influence of the afterbody on the forebody flow. The body cross-section was chosen to be circular to facilitate the fabrication of exchangeable afterbodies, which were made from cylindrical pieces sliced off at the required angle; this resulted in the slanted surfaces being ellipses elongated in the streamwise direction.

**Experimental Arrangement and Measured Quantities** — The tests were conducted in a wind tunnel of the open-return, suck-down type, with test-section dimensions of 500 x 700 mm, maximum velocity of 55 m/sec, and free-stream turbulence intensity u'/U less than 0.1%. The main part of the model was a circular cylinder 254 mm long, with a diameter of 38 mm, suspended in the center of the test-section on six piano

wires 0.35 mm in diameter (Fig. 7). The wires were inclined at 45° to the stream direction in order to suppress vortex shedding and to reduce flow disturbances; Reynolds number based on the wire diameter and on the nominal speed of the experiment was 875. The cylinder was preceded by a slender ogival nose-piece 90 mm long, and its downstream end was capped by interchangeable afterbodies with slanted bases having slant angles from 0° to 70°. Altogether, 17 different slant angles were tested; these were chosen to be at equal increments of 5° (excluding 65°), plus three others with angles of 46.5°, 47.25° and 48.5°.

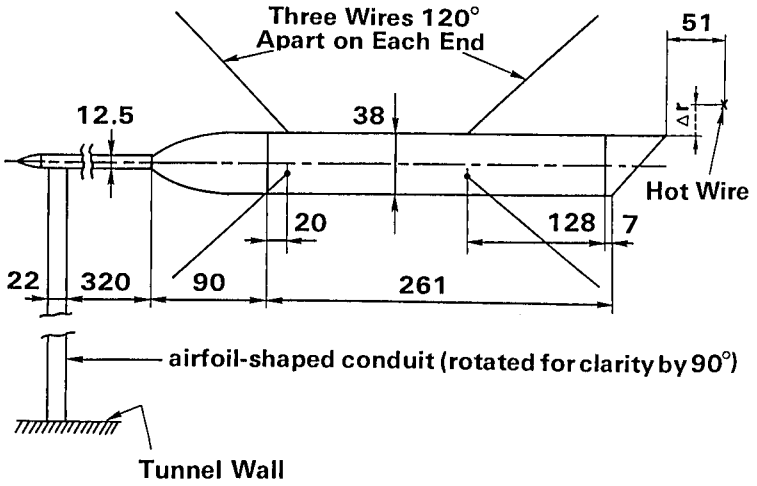


Fig. 7. Experimental arrangement for pressure and hot-wire measurements. Dimensions are in mm.

All tests were run at a nominal speed of 38 m/sec. The boundary layer was turbulent with a momentum thickness, at a point 0.5 diameter ahead of the base, of 0.70 mm ($\theta$/D = 0.018). Reynolds number based on the cylinder diameter was $Re_D$ = 94,000. The suspension system was not entirely rigid on account of suspension-wire elasticity, but its natural frequency was more than an order of magnitude below the forcing (shedding) frequency. No oscillation of the cylinder was observed during runs. Blockage ratio of the cylinder in the wind-tunnel was about 0.3%.

A DISA 55M hot-wire system with one linearized single-wire miniature probe was used to investigate the unsteady properties of the near wake. The hot wire was positioned in the plane-of-symmetry of the base at a distance of 51 mm (1.33 diameters) downstream from the trailing edge. Its lateral position was always on the trailing-edge side of the wake (Fig. 7), at a point where u'/U, when high-pass filtered below a frequency corresponding to $S_D$ = f D/U = 1.0, had a value of 0.5%. This was done to minimize the masking effect of the shear-layer turbulence on the periodic signal ($S_D$ = 0.2 - 0.4). It was reasoned that if the rms of the filtered signal were maintained constant, the hot wire would always be located in about the same

*References pp. 216-217.*

position with respect to the shear-layer edge. As will be discussed later, increasing the base angle tended to turn the wake towards the trailing-edge side, and so this lateral location was not the same for all cases. The hot-wire signal was used to determine whether any regular motions were present in the wake, and to establish their frequency and intensity. To this end the signal was displayed on an oscilloscope for visual inspection, and also simultaneously processed by a narrow-band spectrum analyzer.

Surface static pressure was measured at three locations along a horizontal line placed midway down the slanted surface (Fig. 8). All three taps ended in one cavity, from which a single pressure line was led through the nose extension and a streamlined conduit to a Statham PM5TC pressure transducer. When making pressure measurements from any one tap, the other two were taped over, leaving only the one of interest open.

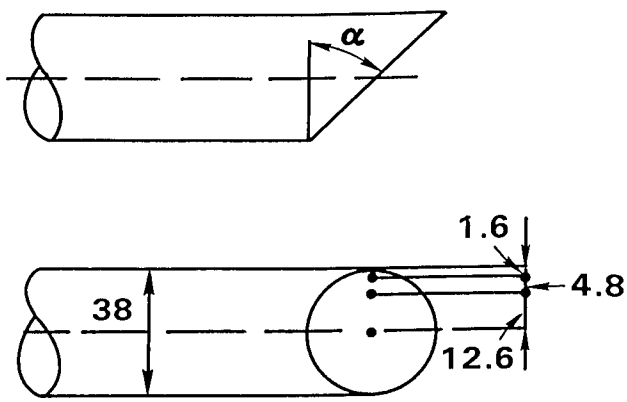


Fig. 8. Location of the three pressure taps on the slanted base. Dimensions are in mm.

Results — *Base Pressure* — The base-pressure development with base slant proved to be very dramatic, and confirmed the expected existence of two widely different base-flow patterns; the changeover occurred on this particular geometry at about 47.5° (Fig. 9). Below 47.5° (Regime I) the base-pressure coefficient was negative and fairly uniform across the base, with a minimum at the centerline tap (#1) and a maximum at the edge tap (#3). The difference between the coefficients at these two taps was about 0.02 at 0°, decreasing to 0.01 at 47.25°. The overall level of base pressure was seen to decrease slightly with increasing $\alpha$ up to 25°, and then was relatively constant. Above 47.5° (Regime II) the base-pressure distribution exhibited sharp pressure gradients across the base, with a maximum pressure at the centerline and a minimum somewhere in-board of the side edges.

The changeover from one flow pattern to another was very abrupt. The original set of end-pieces, manufactured in a sequence with 5° intervals, showed that the pattern

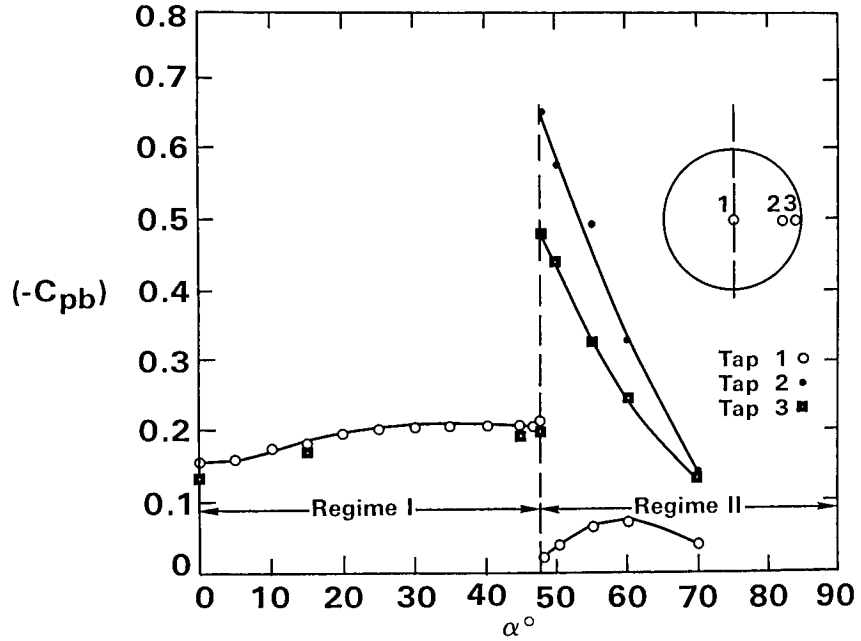


Fig. 9. Base-pressure variation with slant angle.

changeover occurred somewhere between 45° and 50°. To narrow down the interval where the change occurred, two other end-pieces were made with $\alpha$ = 46.5° and 48°. It was expected that one of these two end-pieces would be near enough to the changeover (within 1°) that an intermittent flow behavior would be observed, with the two flow patterns alternating more or less randomly. However, both pieces exhibited very stable flow patterns, 46.5° having the quasi-axisymmetric type (Regime I) and 48° having the 3-D type (Regime II). An even greater surprise was that the flow patterns were so stable that even large perturbations, (e.g., inclination of the whole model at $\pm$5° to the free-stream in either of two perpendicular planes) did not change their basic character. This indicated that each regime was inherently stable and that the changeover must be very abrupt indeed.

As a final step, an afterbody with $\alpha$ = 47.25° was manufactured, allowing the critical angle to be located within 0.375°. This configuration again showed a stable flow pattern, which was of the quasi-axisymmetric type; thus, the changeover was occurring somewhere between 47.25° and 48°. Inclination of this last model, in its plane of symmetry, with respect to the free stream did produce the expected changeover to the 3-D flow pattern. To achieve this it was necessary to incline the model tail downwards by about 5°, making the base angle about 52°. Once the changeover occurred the new pattern was completely stable. Returning the cylinder to the horizontal position did not bring back the original flow pattern; to achieve that, an inclination in the opposite sense by about 1° was required. This means that the flow had a hysteretical behavior over a range of some 6°.

*References pp. 216-217.*

One consequence of increasing the slant angle is an increasingly large projection of the base surface in the transverse direction. Since the base is subjected to a low pressure, there is a force on it acting in that direction. This also means that the flow experiences an equal but opposite force, making it deflect towards the trailing edge of the base; this deflection was actually observed using the hot wire, located as previously described 1.33 diameters downstream, at a lateral position $\Delta r$ where the filtered u'/U = 0.5%. The locus of $\Delta r$ as a function of slant angle is shown in Fig. 10.

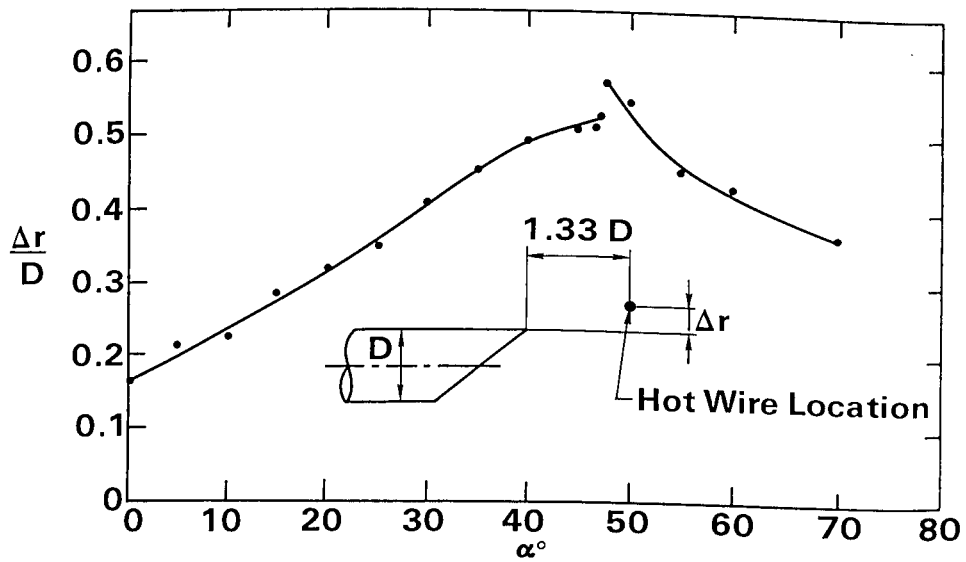


Fig. 10. Lateral location of the point where u'/U, high-pass filtered below $S_D$ = 1.0, equals 0.5%.

*Drag Force* – The axial force on the body (drag) was measured using a different experimental arrangement. Following a suggestion of W. W. Willmarth of the University of Michigan, a pendulum method was used. The cylinder, minus the upstream pressure-line conduit, was suspended on four vertical 0.127 mm wires (two in front and two at the rear). The force on the body was calculated from the observed downstream displacement of the body caused by the air flow, as measured by a micropositioned transit. Good data repeatability (±1% of $C_D$) was obtained using this simple arrangement.

The data obtained by the pendulum technique are presented in Fig. 11. In Regime I the $C_D$ rose gradually with $\alpha$, increasing by 0.06 from $\alpha$ = 0° to $\alpha$ = 45°. The magnitude of this change is close to that observed in the base pressure (Fig. 9), as may have been expected since the base pressure, which is the only source of the drag increase, was fairly uniform across the base. Changeover to Regime II, at the critical angle, produced a dramatic increase in $C_D$. The total body drag increased by an

impressive jump of $\Delta C_D = 0.325$ to more than double its value! Further increase in $\alpha$ gave a sharp drop in $C_D$, leading to values lower than the zero-slant drag beyond $\alpha \approx 69°$.

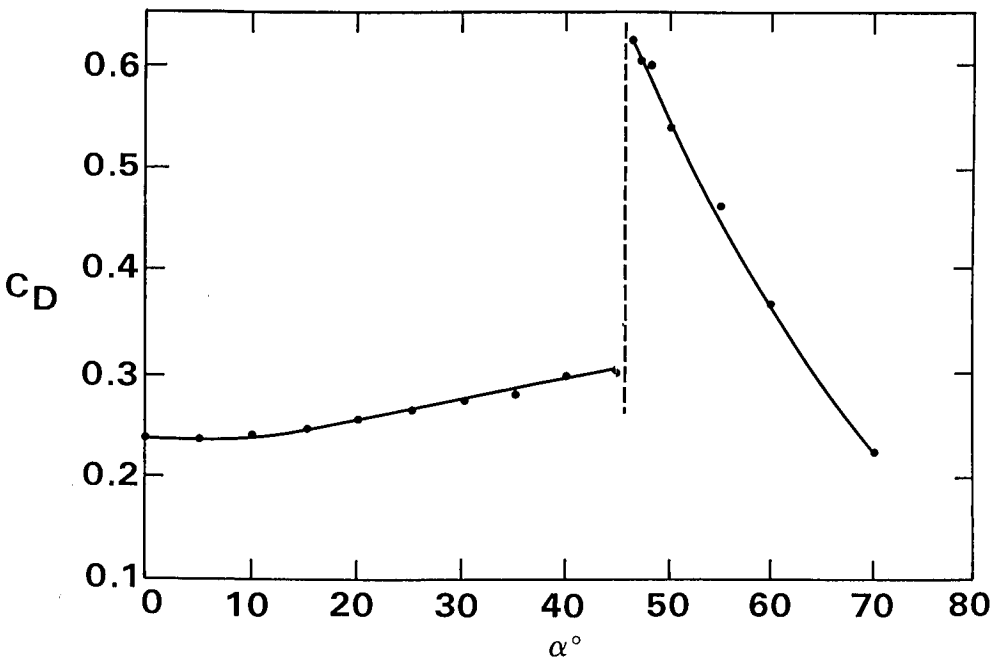


Fig. 11. Drag-coefficient variation with slant angle.

It is interesting to note that the jump from one regime to another occurred in this case between $\alpha = 45°$ and 46.5°, rather than between 47.25° and 48° as in the case of the pressure runs, a difference of some 2°. In both cases the body was placed in the test section in the same position and was aligned with respect to the same reference points. The only differences were in the suspending wires and in the pressure-line conduit, and this was apparently sufficient to produce the difference in the critical angle.

*Wake Periodicity* – Slanting the base from its original, vertical, position greatly increased the shedding intensity. In the vertical (0°) position, the near-wake hot-wire signal showed only weak signs of periodicity (Fig. 12), but the spectrum had a definite peak, and the hot-wire signal itself began to show a progressively better-defined periodicity. The spectral peak was highest and sharpest at $\alpha = 20°$; beyond this angle it decreased and broadened at the same time (Fig. 13b).The total intensity of the spectral "hump" increased up to about $\alpha = 30°$ (Fig. 14), where the hot-wire trace gave a very clear indication of a significant degree of regularity.

*References pp. 216-217.*

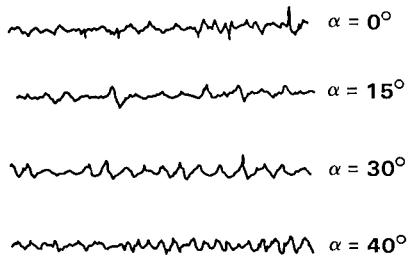


Fig. 12. Velocity traces for several different slant angles.

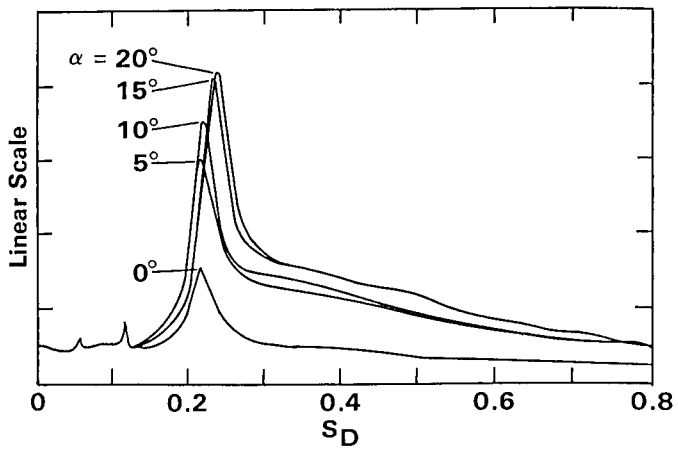


Fig. 13a. Velocity spectra at $\alpha$ = 0°-20°. Linear vertical scale.

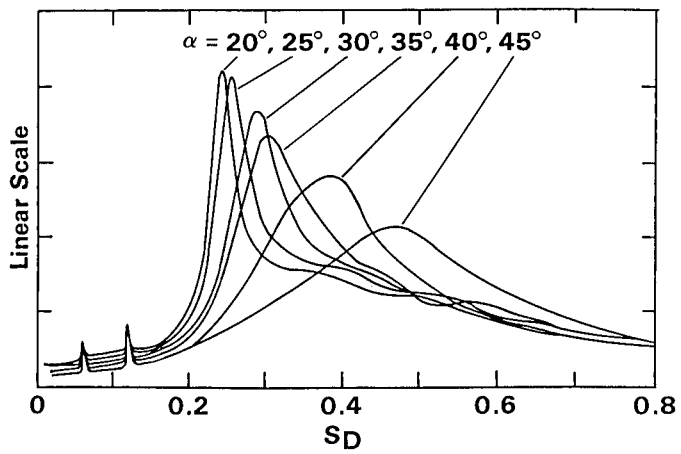


Fig. 13b. Velocity spectra at $\alpha$ = 20°-45°. Linear vertical scale.

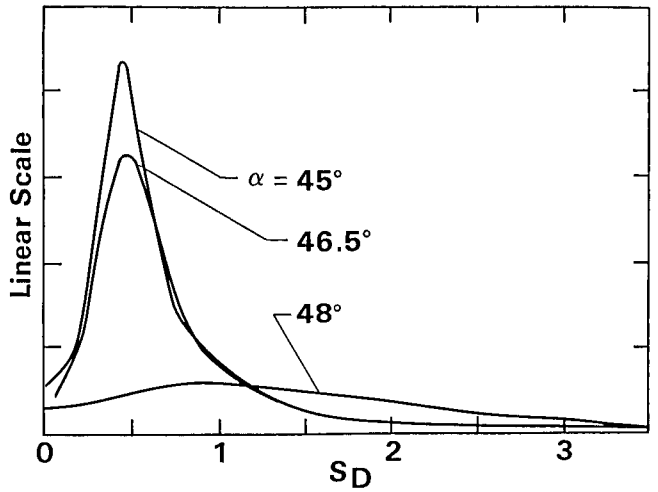


Fig. 13c Velocity spectra near the critical slant angle, $\alpha$ = 45°-48°.Linear vertical scale; note the change in the horizontal scale and in the slant angle increments.

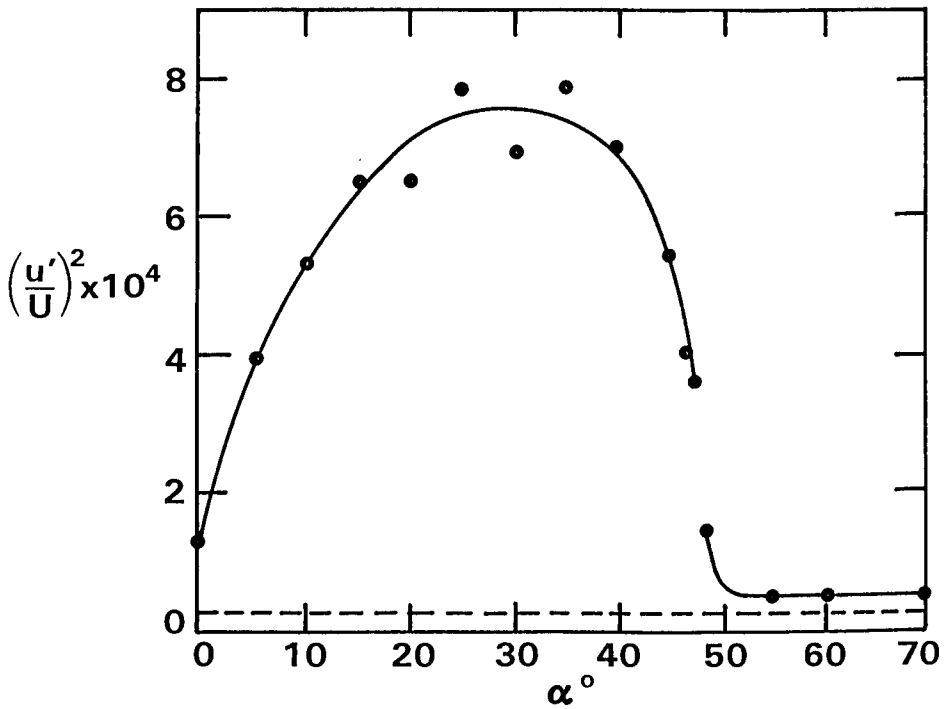


Fig. 14. Fluctuation intensity $(u'/U)^2$ vs. slant angle. —Total intensity, ----intensity of the filtered signal.

*References pp. 216-217.*

The Strouhal number associated with the mid-point of the spectral hump exhibited a monotonic increase with slant angle, and in the vicinity of the changeover point had a magnitude more than double that at 0° (Fig. 15). Above the critical angle after the change in base-flow regime occurred, no regular shedding was visually detectable in the hot-wire signal, though the spectra for $\alpha = 48 - 55°$ still showed a spectral hump which was very broad and was centered around $S_D \approx 1.25$ (Fig. 13c). The magnitude of this hump decreased rapidly with $\alpha$, and at 55° it was almost undetectable.

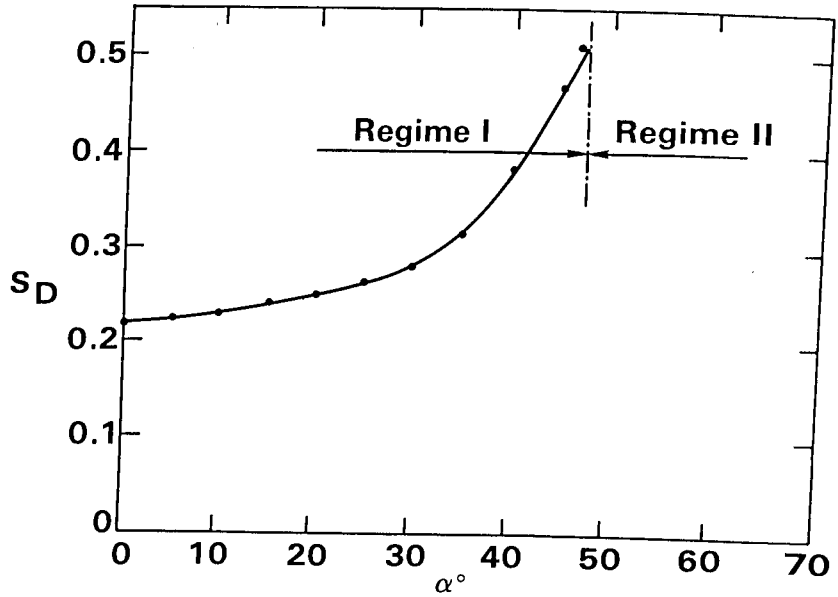


Fig. 15. Effect of slant angle on the shedding frequency (Strouhal number).

Discussion — The change in the slanted-surface pressure distribution at the critical angle is consistent with the proposed model of the flow behavior (Fig. 6). The pressure uniformity across the base in Regime I would be expected for the quasi-axisymmetric flow pattern. Similarly, the pressure distribution in Regime II agrees with what was expected; the large increase in centerline pressure is an indication of a tendency towards flow reattachment in the mid-portion of the base, while the very low pressure near the edge is due to the close proximity of a concentrated streamwise vortex rolling up off the side edge, in a fashion similar to that sketched in Fig. 6b.

Prior to the experiment it was expected that the flow pattern changeover would take place over a range of $\alpha$, within which an intermittent switching back and forth between the two regimes would be taking place, as observed in the Janssen & Hucho experiment. The actual data proved to be a surprise as they showed the two patterns to be very stable. In fact, this observed stability was so strong that both patterns could exist and be completely stable on the same body ($\alpha = 47.25°$).

The basic experiment on the circular cylinder served well its purpose. It demonstrated the existence of two dramatically different separation patterns, one of which, the highly three-dimensional one, has the capability of large drag generation. At the critical slant angle the drag difference between the two patterns can be very large, giving this flow phenomenon and its understanding great practical importance. Another interesting effect of slant angle is its role in promoting near-wake periodicity. At slant angles around $\alpha = 30°$ the periodic motions in the near wake are much more pronounced in intensity than at 0°, and may cause significant periodic loading on the rear portion of a body. This effect is worth further study, as it may possibly couple with the natural frequency of the body's suspension system. (On an automobile traveling at typical highway speeds, the shedding frequency should be in the range of 3-6 Hz.)

## VEHICLE-LIKE BODY NEAR AND AWAY FROM THE GROUND

The first experiment left unanswered two major questions: Are these results transferable to vehicle-like shapes, and what is the effect of ground proximity on the critical angle and drag overshoot? To provide the answers, a further experiment was conducted. The tested body had vehicle-like proportions (Fig. 16), with dimensions of 900 x 405 x 270 mm, i.e., length:width:height ratio of 3.33:1.50:1.00. The body was again equipped with interchangeable bases of various slant angles, but this time the area of the slanted surface (as well as its aspect ratio) was kept constant. This meant that the vortex-sheet-generating edge was of the same length ($L_S$ = H, see Fig. 16) at all slant angles. The volume of the body was also kept constant, both to preserve the interior volume (a factor in road-vehicle applications) and to keep constant the effective length $L_{eff}$ = volume/(W x H). This required lengthening the body's bottom surface at non-zero slant angles; the maximum elongation needed, at $\alpha = 45°$, was 67.5 mm or about seven percent.

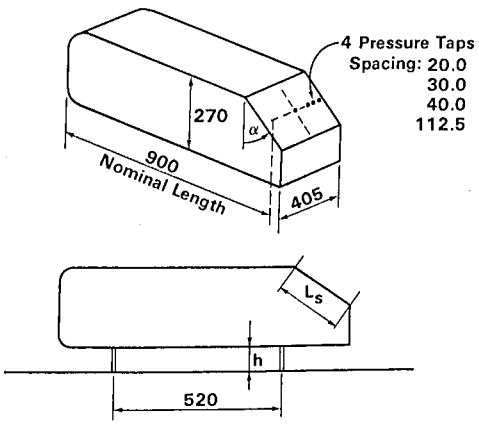


Fig. 16. Experimental arrangement for the vehicle-like body. Dimensions are in mm.

*References pp. 216-217.*

Two different heights above the ground were used, one to simulate a free-stream situation and one typical of a road vehicle. In terms of an equivalent diameter ($D_{eq} = \sqrt{4\,WH/\pi} = 373$ mm), the dimensionless ground clearances were $h/D_{eq} = 0.82$ and 0.12, respectively. The former value was chosen to be beyond the height where ground proximity starts to affect the force characteristics of this type of body.

**Experimental Arrangement and Measured Quantities** – The second experiment was conducted in a vehicle-aerodynamic wind tunnel used for partial-scale-model testing (Mason, Beebe & Schenkel, 1973). This facility is of the closed-path type, and is equipped with a free-standing test-section floor, which acts as a ground plane. Test-section dimensions are 1400 x 4570 mm; it has a maximum velocity of 256 km/h and a turbulence level u'/U = 0.3%.

The model was suspended on two cylindrical stilts 15.9 mm in diameter. There were 19 different afterbodies, with slant angles between 0° and 85° (note that 90° is identical to 0°), which were spaced 10° apart in regions of lesser importance, but 5° and 2.5° apart in regions where rapid changes were occurring.

All tests were run at a nominal speed of 58 m/sec, giving a Reynolds number based on equivalent diameter of $1.4 \times 10^6$, or about 15 times that of the first experiment. Stilt Reynolds number was about 60,000, i.e., subcritical. Blockage ratio of the model at zero yaw was 1.7%.

Surface static pressure was measured at four locations across a line midway down the slanted surface (Fig. 16). In addition, all six forces and moments were measured using a strain-gage force balance to which the support stilts were anchored. Flow visualization using surface tufts, smoke and a vortex paddle-wheel were used to identify the near-wake flow patterns and to document their nature.

**Results** – *Drag and Lift* – The drag data was corrected for the tare drag of the stilts (both drag and lift coefficients are based on the body frontal area). In the data taken away from the ground (Fig. 17) one can observe trends very similar to those found in the first experiment; however, the critical angle shifted from 47° to 60°. In Regime I drag showed a slight increase ($\Delta C_D = 0.03$) with slant angle, followed by a sudden increase of $\Delta C_D = 0.16$ at the critical angle. Beyond this angle $C_D$ dropped very rapidly, reaching a minimum at about $\alpha = 82°$, which was 0.21 below the maximum and about 0.03 below the zero-slant value. The drag decrease from $\alpha = 90°$ to 82° is apparently a type of boat-tail effect which, below 82°, is overpowered by the growing strength of the edge vortices. Lift data (Fig. 18) have an even more pronounced variation with $\alpha$ than the drag data. The fact that $C_L$ was positive at all non-zero slant angles was expected, as the slant exposes an upward projection of the low-pressure afterbody surface. However, the magnitude of the lift coefficient variation was unexpected. Near the critical angle the maximum $C_L$ exceeded greatly the maximum $C_D$, making the model a lifting body in that range (i.e., $C_L/C_D > 1$).

Drag-coefficient trends near the ground (Fig. 19) were quite similar to the free-stream trends, but the magnitude of $C_D$ variations with the slant angle was smaller. The critical angle was the same as for the free-stream case. At $\alpha = 0°$ the drag coefficient was slightly higher than in the free stream, by 0.025. The drag rise in Regime I was less pronounced and the jump to Regime II at the critical angle was

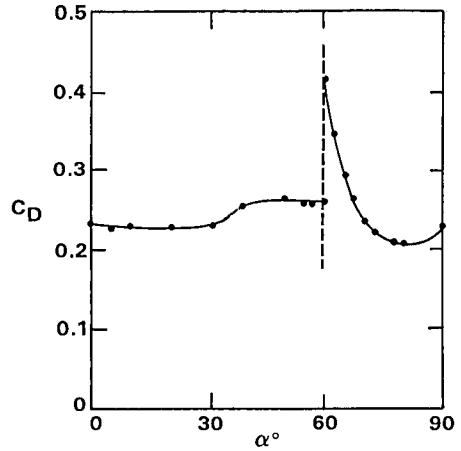


Fig. 17. Drag-coefficient variation with slant angle, $h/D_{eq} = 0.82$ (free stream). Data corrected for drag of stilts.

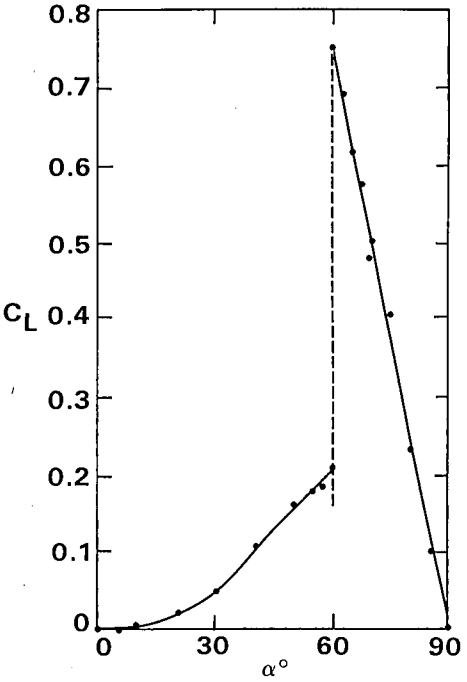


Fig. 18. Lift-coefficient variation with slant angle, $h/D_{eq} = 0.82$ (free stream).

*References pp. 216-217.*

only $\Delta C_D = 0.11$. The subsequent decrease to the minimum at $\alpha = 80°$ was $\Delta C_D = 0.155$. The trends of data of Janssen & Hucho (1974), drawn in a broken line for comparison, are seen to be in general agreement with the present results. The lift coefficient (Fig. 20) behaved very similarly to the free-stream case; in fact, Fig. 18 and Fig. 20 differ for the most part only by a constant vertical shift of $\Delta C_L = 0.2$.

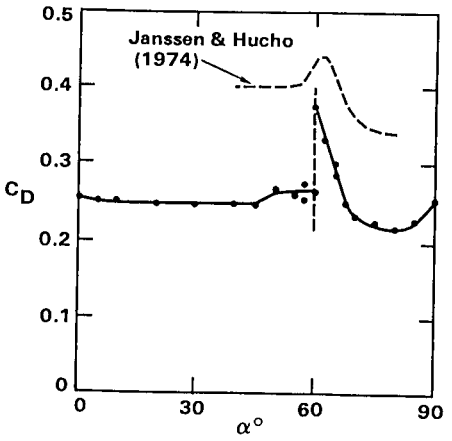


Fig. 19. Drag-coefficient variation with slant angle, $h/D_{eq} = 0.12$. Data corrected for drag of stilts.

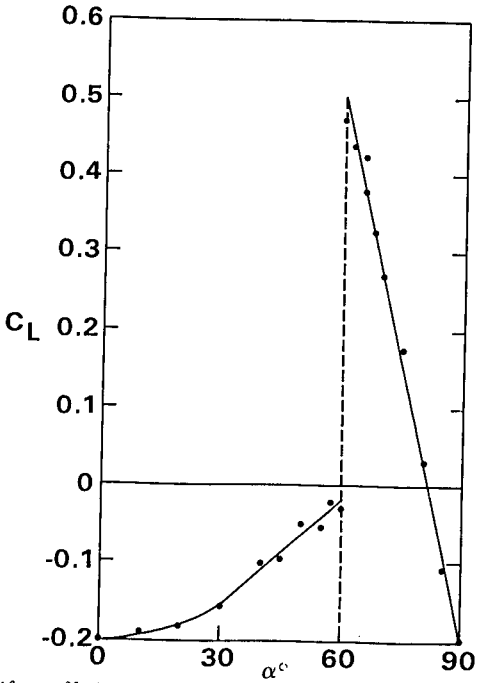


Fig. 20. Lift-coefficient variation with the slant angle, $h/D_{eq} = 0.12$.

*Flow-Visualization* — Flow visualization, through three different techniques, was used to study the nature of the two flow patterns near the critical angle. Flow at the body surface was explored by the use of tufts. Below the critical angle the slanted-surface flow was seen to be entirely separated, and the tufts on the sides of the body were quite well aligned with the free-stream direction. At $\alpha = 65°$, above $\alpha_{crit}$, the upper third of the slanted surface showed signs of flow separation, but the lower two-thirds clearly had an attached flow. The tufts along the sides of the body were inclined upwards towards the slanted side edges due to cross flows from the sides onto the slanted base, indicating a presence of very low pressures near the side edges.

The wake was also probed with a vortex-paddle-wheel (25 mm in diameter) in an effort to compare the strength of streamwise vortex motions and to map their

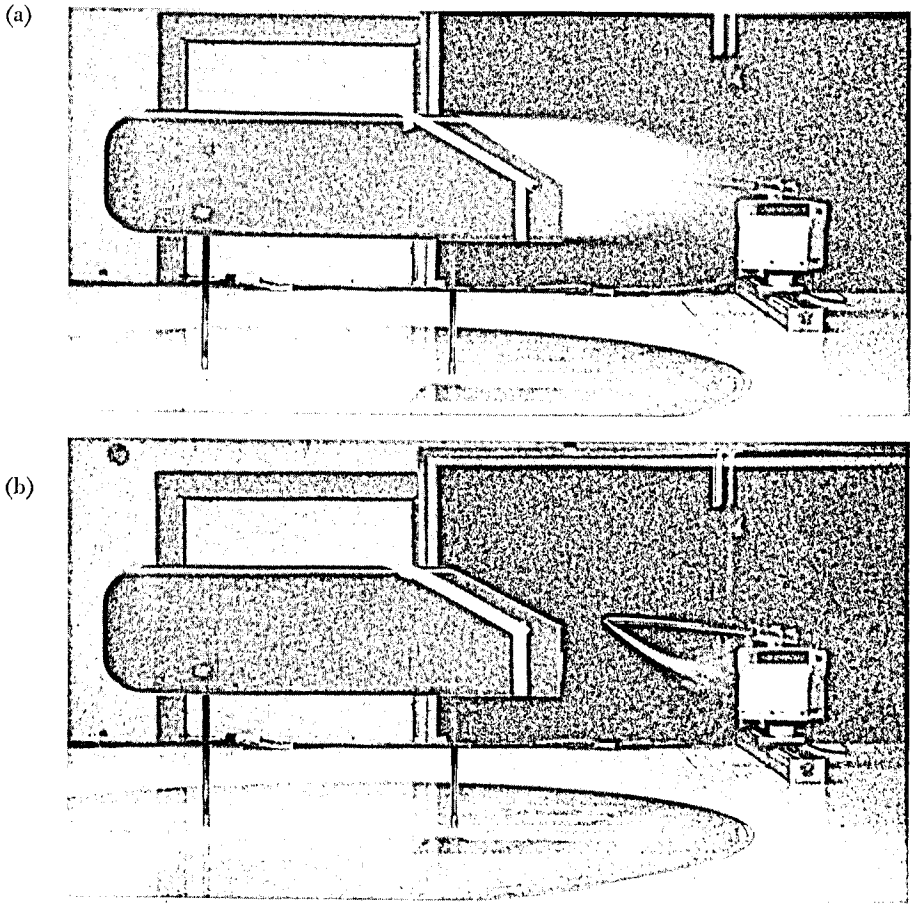


Fig. 21. Smoke visualization of the near wake, (a) $\alpha = 57.5°$, (b) $\alpha = 62.5°$. Point of smoke release is located on the body centerline, and in both photographs is in about the same position with respect to the base.

*References pp. 216-217.*

trajectory. The difference between the two patterns was very striking; while there was almost no vortex activity below $\alpha_{crit}$, above it ($\alpha$ = 62.5°) two very strong vortices were observed. These vortices were approximately aligned with the two side edges, deviating from them by some 5-10° upward (away from the surface) and inward (towards the centerline).

Smoke visualization of the near wake displayed clearly the very different nature of the two flow regimes. In Regime I ($\alpha$ = 57.5°, Fig. 21a) the smoke showed a typical separated bubble, much like what one would expect behind a vertical base. In Regime II ($\alpha$ = 62.5°, Fig. 21b) one could see a strong downwash and no sign of separation. In both photographs the smoke probe was located on the body centerline in the same position with respect to the base. Moving the smoke probe sideways away from the plane of symmetry produced little change in the smoke behavior in Regime I, but in Regime II one could observe strong swirling motions near the body edges.

*Slanted-Surface Pressure* — Slanted-surface pressure data also showed the difference in the two regimes — a relatively uniform pressure in Regime I and a pronounced lateral variation in Regime II. This fact is well illustrated in Fig. 22, showing the two possible bi-stable pressure patterns recorded on the same (critical) afterbody placed near the ground. The two pressure curves complement the flow visualization pictures of Fig. 21, by showing the types of pressure distribution associated with the two smoke photographs. A comparison of the two figures also makes one realize that conventional visualization, using smoke released along the centerline, tends to encourage two-dimensional thinking, which may be quite misleading. In the case at hand, the smoke pictures suggest that the attached flow in Regime II means an increase in the base pressure as compared to Regime I. The pressure data show, however, that just the opposite is true.

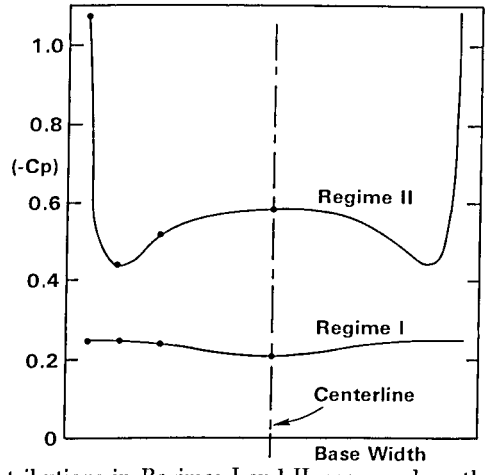


Fig. 22. Pressure distributions in Regimes I and II, measured on the same base with a 60° slant angle, at $h/D_{eq}$ = 0.12. Pressure taps were placed on a horizontal line across the base, located midway down the base.

**Discussion** — The results obtained for the vehicle-like body were in general agreement with the cylinder experiment, but there were important differences, the most striking of which was in the value of $\alpha_{crit}$, which was 60° instead of 47°. There were several important geometrical differences between the two models, e.g., a circular compared to a rectangular cross-section, but we believe that the main reason for the critical-angle shift was the change in the aspect ratio of the slanted surface. At 47° the base of the cylinder was an ellipse with AR = 0.68, while the rectangular body had AR = 1.5. The direction in which the critical angle changed with AR is consistent with the following reasoning. As AR increases, the effect of the side-edge vortices on the overall flow patterns gets progressively smaller, as only a relatively small portion of the base is exposed to them. Thus, the attached flow patterns, supported by inflow from the body sides which passes over the edge vortices, breaks down at larger and larger values of $\alpha$ (i.e., when the slanted surface is more closely aligned with the external flow). Also, as the relative importance of the edge vortices decreases with increasing AR, the value of the drag overshoot may be expected to decrease and this effect is probably at least partly responsible for the smaller jump in $C_D$ at the critical angle, $\Delta C_D = 0.16$ for the rectangular body vs. 0.325 for the cylinder.

The effect of ground clearance (for the chosen clearance of $h/D_{eq} = 0.12$) was less important. The value of the critical angle appeared to be unchanged, but the variation in $C_D$ with $\alpha$ was somewhat reduced. The shape of the lift-coefficient curve was affected only very little by ground proximity, which was a surprise, as lift would be expected to be very sensitive to ground clearance.

An important difference between the two bodies was in the stability of the two regimes. The vehicle-like body had less-stable flow in the vicinity of the critical angle; especially near the ground the force and pressure coefficients were not exactly repeatable. At $\alpha = 60°$ one could obtain either of the two flow patterns by yawing the model sufficiently far away from, and then returning to, the head-on position.

An interesting observation may be made concerning the slope of the almost-linear lift curve in Regime II. The slope of this curve $(-\partial C_L/\partial \alpha)$ is about 1.43 for the free-stream case and about 1.33 for the case near the ground. These numbers may be compared to the data for rectangular flat plates inclined with respect to a free stream. Interpolating the data presented by Lamar (1974), one obtains for AR = 1.5 a lift coefficient slope of about 2.35. Thus, the bluff and bulky block at zero angle of attack, but with a slanted rear surface, had fully 60% of the lift slope of a flat plate of the same size as the slanted surface. Furthermore, the lift-to-drag ratio for the bluff body at $\alpha_{crit}$ was only four percent less than for the flat plate.

## CONCLUSIONS

1. Slanting the rear surface of a simple bluff-ended body away from the normal to the streamwise direction affects strongly its drag. The drag curve develops a

*References pp. 216-217.*

pronounced local overshoot (a bulge) over a relatively narrow range of slant angles, with a drag maximum at a "critical angle."

2. Base-pressure data and flow visualization show clearly that there are two very different separation patterns that can exist in the near wake. Below the critical slant angle a quasi-axisymmetric separation pattern is established (Regime I), while above it there is a 3-D separation pattern with two pronounced streamwise vortices forming on the side edges of the slanted surface (Regime II).

3. In Regime II, base slant tends to make a bluff-body a lifting body. For the vehicle-like body studied here, the slope $(-\partial C_L/\partial \alpha)$ of the lift coefficient curve (based on the area of the slanted surface) was 1.43 when the body was away from the ground, and 1.33 near the ground. The former value constitutes a full 60% of the lift slope measured for rectangular flat plates of the same aspect ratio as that of the slanted surface. The lift force has a maximum at the critical slant angle, where it may reach magnitudes larger than the drag force. In the case of road vehicles this means that a very sizeable rear-axle lift can be generated by improper roof (or window) slant.

4. The circular-cylinder data show that in Regime I base slant produces an increase in base-flow unsteadiness, dominated by quasi-periodic vortex shedding at a Strouhal number of 0.2 - 0.4.The increased intensity means increased transverse periodic loads, and they may couple with the natural frequencies of a body suspension system. The only data available are those obtained away from ground; therefore, a study of ground effect on shedding is needed in order to assess its importance to road vehicles.

5. The effect of the aspect ratio (AR) of a slanted surface on the critical phenomenon appears to be two-fold: First, increasing AR increases the value of the critical slant angle; second, AR has a strong effect on the magnitude of the drag overshoot.

6. The tests have indicated that ground proximity does not greatly affect the value of $\alpha_{crit}$, but it tends to reduce the magnitude of the $C_D$ variation with $\alpha$. The trend of $C_L$ with $\alpha$ (the lift slope)was unaffected by ground proximity, but the absolute value of $C_L$ was lowered by a constant amount.

## REFERENCES

*Nash, J. F., Quincey, V. G. & Callinan, J. (1963), Experiments on Two-Dimensional Base Flow at Subsonic and Transonic Speeds, ARC R&M No. 3427, p. 17.*

*Bearman, P. W. & Trueman, D. M. (1972), An Investigation of the Flow Around Rectangular Cylinders, The Aeronautical Quarterly, Vol. XXIII, pp. 229-237.*

*Janssen, L. J. & Hucho, W.-H. (1974), Aerodynamische Formoptimierung der Typen VW-Golf und VW-Scirocco,* **Kolloquium ueber Industrie-aerodynamik,** *Aachen, Part 3, pp. 46-69.*

*Lamar, J. E. (1974), Extension of Leading Edge Suction Analogy to Wings with Separated Flow Around the Side Edges at Subsonic Speeds, NASA TR R-428, pp. 48 and 53-57.*

*Mair, W. A. (1965), The Effect of a Rear-Mounted Disk on the Drag of a Blunt-Based Body of*

*Revolution, The Aeronautical Quarterly, Vol. XVI, pp. 350-360.*

*Mair, W. A. (1969), Reduction of Base Drag by Boat-Tailed Afterbodies in Low-Speed Flow, The Aeronautical Quarterly, Vol. XX, pp. 307-320.*

*Mason, W. T., Jr., Beebe, P. S. & Schenkel, F. K. (1973), An Aerodynamic Test Facility for Scale-Model Automobiles, SAE Paper No. 730238.*

*Nakaguchi, H., Hashimoto, K. & Muto, S. (1968), An Experimental Study on Aerodynamic Drag of Rectangular Cylinders, Journal of the Japan Soc. of Aeronautical and Space Sciences, Vol. 16, pp. 1-5.*

## DISCUSSION

*Prepared Discussion*

**J. E. Hackett** *(Lockheed-Georgia Company)*

This is on behalf of Professor Rainbird. He would like to point out the similarity between the flows which have just been described and the flow on the upswept fuselage of an airplane. Both the Canadians and Lockheed use transport aircraft in which the aft end of the fuselage is upswept. This is pretty much the upside down of what we have just been talking about with respect to cars. Regime II is generally found in these cases because the upsweep is fairly modest, although, of course, there is a downwash field from the wings which tends to add to the cross-flow effects. Flows of this type have been studied quite widely by Peake.* The surface flow is very complex, and measurements of pressure distributions need to be very detailed indeed in order to make sense of what's going on. Another point that Professor Rainbird asked me to make was the fact that there has been some work done in Japan on semisubmerged ships** which showed very similar types of flows at the aft end of the ships. Studies have been done of the vorticity in the wake behind them, which is a valuable aid to interpretation.

My personal comments . . . I feel that it should be possible to get a much better understanding of how the drag occurs on a car by doing good wake traverses. I think it would be most useful to separate out the losses in total pressure; for example, to identify the viscous losses as opposed to the vortex losses - I don't like the term induced drag in this context. I think it would be possible to measure the cross flows (we've been doing some of this at Lockheed) and identify separately the vortex drag. Separate these two items and, hopefully, at some stage it ought to be possible to establish the drag floor for automobiles, because there does not have to be any vortex drag if cars are brought right down to the ground and the pressure distributions are suitably arranged. You don't have to have vortex drag! Practical considerations are

---

**Peake, D. J. (1976), Controlled and Uncontrolled Flow Separation in Three Dimensions, National Aeronautical Establishment, Ottawa, Aeronautical Report LR591.*

***Tanaka, H. (1974), A Study of Resistance of Shallow-Running Flat Submerged Bodies, Journal of the Society of Naval Architects of Japan, Vol. 136.*